AGRIMARO.Q, A Service Robot for Precision Agriculture in Greenhouses

# AGRIMARO.Q, A Service Robot for Precision Agriculture in Greenhouses

Giovanni Colucci[0000-0002-2996-9013] [1], Andrea Botta[1], Luigi Tagliavini[1], Lorenzo Baglieri[1], Simone Duretto[1] and Giuseppe Quaglia[1]

[1] Politecnico di Torino
Department of Mechanical and Aerospace Engineering
{giovanni_colucci, andrea.botta, luigi.tagliavini, lorenzo.baglieri, simone.duretto, giuseppe.quaglia}@polito.it

**Abstract.** The paper presents a novel mobile robot for Precision Agriculture in protected cultivation, named AGRIMARO.Q (AGRIcultural MAte RObot) mainly characterized by a pseudo-omnidirectional mobility by means of three swerve drive units and an adjustable track. After presenting the robot design mainly in terms of track adjustment mechanism and wheel swerve drive sub-systems, the paper focuses on the kinematic model of the robot along with final considerations about its mobility in application cases.

**Keywords:** Precision Agriculture, Protected Cultivation, Pseudo-Omnidirectional Service Robot, Kinematic Modelling

## 1 Introduction

Precision Agriculture applies innovative technologies to traditional farming, often constrained by manual labor and limited data [1]. Robotic solutions have emerged to address labor shortages and global food market competition [2], particularly in protected cultivation. These service robots, ranging from prototypes to commercial products, monitor, interact with crops, and perform tasks like weeding, fertilize, harvesting and sampling. Notably, Arad et al. [3] developed a scissor-lift platform for sweet pepper harvesting, while Lehnert et al. [4] and Birrell et al. [5] proposed designs for similar tasks.

Additionally, platforms like Thorvald II [6] offer versatility and mobility with swerve drive units. These flexible robotic platforms can adapt to diverse environments and perform various tasks, making them highly promising in the agriculturally diverse scenario. Moreover, the Thorvald platform mobility when navigating is remarkably determined by the employment of swerve drive units (SWD), meaning that each wheel in contact with the ground is a drive unit which can also. The flexibility of the Thorvald platform is expressed in terms of different designs and solutions, which derive from the same core design but are adjusted to fit a specific application. A noteworthy version of

the Thorvald platform presents a reconfigurable chassis that allows a variable track dimension, that can be modified manually before using the platform.

The current state of the art reveals that modular and adaptable robotic solutions can offer distinct advantages, especially when equipped with swerve drive units that enhance the platform mobility [6], but the use of a high number of SWD units may increase the platform cost together with its overall weight. In response to this, the paper introduces the AGRIMARO.Q mobile robot, whose design takes advantage of a limited number of SWD units and a reconfigurable gantry structure that allows the automatic reconfiguration of the chassis track. The latter feature may be helpful when the robot has to switch between cultivation with different row widths.

## 2 Robot Design

The AGRIMARO.Q robot concept consists of a triangle-shaped gantry structure provided by three swerve-drive units positioned at each triangle vertexes $P_1$, $P_2$ and $P_3$, as depicted in Fig. 1(a). The robot overall dimensions, especially in terms of track size $t$, has been derived from its typical application case, i.e. protected cultivation of fruits and vegetables of small-medium size, also considering alternative scenarios where the gantry structure encompasses more than a single crop row. The final range of $t \in [800, 1200]$ mm was thus associated with a wheelbase length of $w = 1000$ mm to provide enough stability and space for the auxiliary components, such as batteries, a control unit, sensors, and other tools. Fig. 1(b) shows a 3D model of AGRIMARO.Q and its main mechanical subsystems, i.e. the custom swerve drive unit, the track adjustment mechanism and the chassis made of aluminum tubes and clamps, which makes any eventual modification and adjustment relatively easy to do. As a possible use case, the render shows AGRIMARO.Q equipped with a commercial solid fertilizer dispenser.

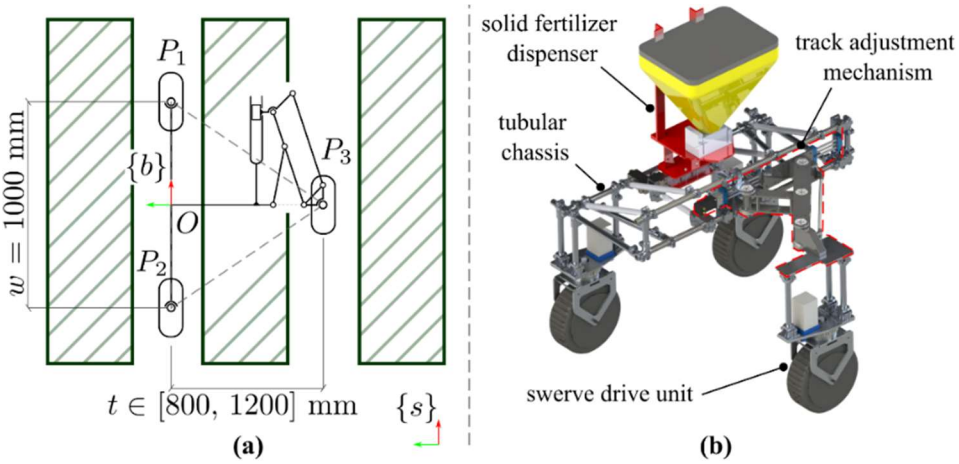


**Fig. 1. (a)** Top view of AGRIMARO.Q robot functional model while navigating among the crop rows. **(b)** AGRIMARO.Q 3D model.

Regarding the drive wheel unit, whose exploded view is depicted in Fig. 2(a), its custom design includes the off-road KN6104 (UUMOTOR) commercial drive unit, whose fork can rotate with respect to the AGRIMARO.Q chassis by means of a hinge steering joint driven by an electric NEMA34 stepper motor (IGUS). Besides, the inclusion of a commercial slip ring between the two parts in relative motion ensures no physical joint limits on the rotation of the steering axis in both directions. The track adjustment mechanism, as shown in Fig. 2(b), is based on a Scott-Russell mechanism provided with a parallelogram to keep the $CC'P_3$ link orientation fixed with respect to the body frame. Among the straight-line mechanism category, this mechanism provides an exact straight-line motion of $P_3$, thus always leading to an isosceles triangle $P_1$, $P_2$, $P_3$, and a good trade-off between a limited number of kinematic joints and a compact geometry, as compared for instance to the four-bar scissor mechanism, the five-bar translating linkage or the Hoeken approximated straight-line mechanism [7]. The figure also shows the final mechanism design, that is constructed on two parallel planes, with exceptions for specific elements such as the actuation subsystem and links C and D. The mechanism is driven by a linear guide, powered by a commercial stepper motor.

## 3 Kinematic Modelling

Fig. 3 represents the top-view of the robot functional diagram. $\{s\}$ is an inertial reference frame, $\{b\}$ is the body one. The figure also depicts the track adjustment mechanism that allow the track length $t$ within the range [800 1200] mm. Let's the two values $[\delta_i, \theta_i]$ respectively be the $i$-th swerve drive unit steering angle and wheel angular rotation along its own rotation axis. Thus, the command vector $\boldsymbol{q}$ of the robot can be described as:

$$\boldsymbol{q} = [\boldsymbol{q_1}, \boldsymbol{q_2}, \boldsymbol{q_3}]^T \quad \text{with} \quad \boldsymbol{q_i} = [\delta_i, \theta_i]^T \tag{1}$$

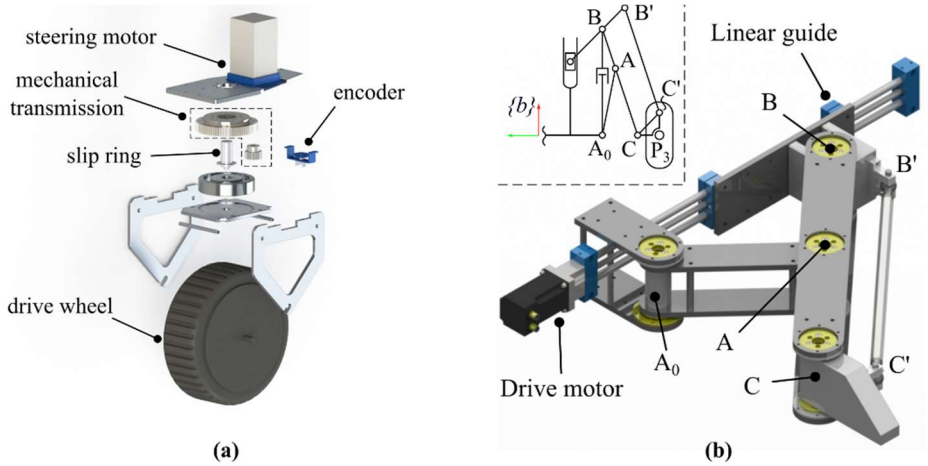


**Fig. 2. (a)** SW unit exploded view. **(b)** Track adjustment mechanism final design.

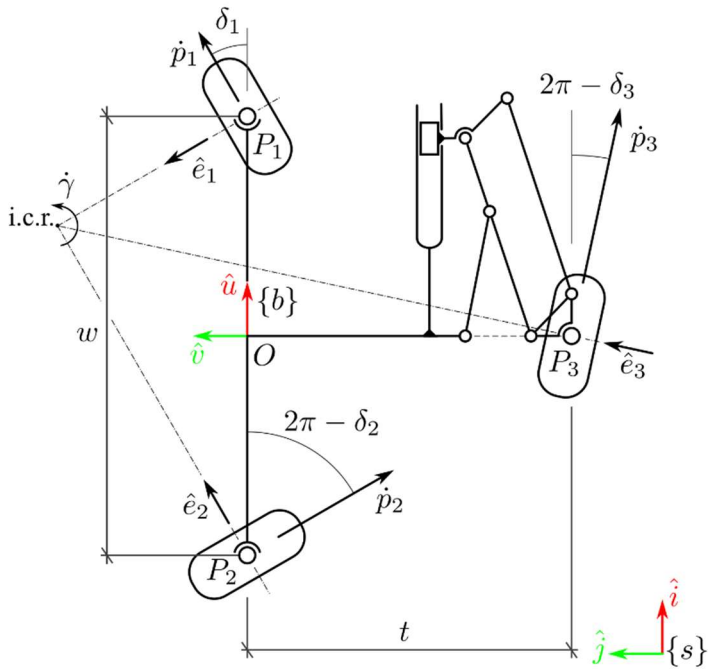


**Fig. 3.** AGRIMARO.Q kinematic model within the $< \hat{\imath}, \hat{\jmath} >$ plane with respect to the fixed reference frame $\{s\}$. Reference frame $\{b\}$ is attached to the robot chassis in point O.

Under the assumption of planar motion, i.e. no linear motion along $\hat{k}$ and no rotations along $\hat{\imath}$ or $\hat{\jmath}$ are allowed, the robot chassis motion can be described in terms of the space velocity twist vector $\boldsymbol{V_b} = [\dot{\gamma}_b, \dot{x}_b, \dot{y}_b]^T$, expressed relative to the body frame $\{b\}$.

The mapping between $\boldsymbol{q}$ and $\boldsymbol{V_b}$ can be developed under the additional simplifying assumption of pure-rolling constraint on the wheel-ground contact, for the velocity of the $i$-th swerve drive wheel center is straightforward to compute:

$$\dot{\boldsymbol{p}}_{\boldsymbol{i}} = \boldsymbol{\omega_i} \times \boldsymbol{r_i} \tag{2}$$

where $\boldsymbol{\omega_i} = \dot{\theta}_\iota \, \hat{\boldsymbol{e}}_{\boldsymbol{i}}$ and $\boldsymbol{r_i}$ is the directional vector from the wheel-ground contact point to the wheel center. Eqn. 2 can be rewritten with $\hat{\boldsymbol{e}}_{\boldsymbol{i}} = \sin(\delta_i)\, \hat{\boldsymbol{u}} + \cos(\delta_i)\, \hat{\boldsymbol{v}}$ and $\boldsymbol{r_i} = r\hat{\boldsymbol{w}}$, where the wheel radius is here assumed as identical for all the three drive wheels:

$$\dot{\boldsymbol{p}}_{\boldsymbol{i}} = \begin{bmatrix} r\cos(\delta_i) \\ r\sin(\delta_i) \end{bmatrix} \dot{\theta}_i = \boldsymbol{s_i}(\delta_i)\, \dot{\theta}_i \tag{3}$$

The same physical quantity can be referred to $\boldsymbol{V_b}$ since the chassis is a rigid body:

$$\dot{\boldsymbol{p}}_{\boldsymbol{i}} = \dot{\boldsymbol{p}} + \dot{\gamma}\, \hat{\boldsymbol{w}} \times \boldsymbol{p}_{\boldsymbol{P_1}} = \begin{bmatrix} \dot{x}_b - y_i\, \dot{\gamma}_b \\ \dot{y}_b + x_i\, \dot{\gamma}_b \end{bmatrix} = \begin{bmatrix} -y_i & 1 & 0 \\ x_i & 0 & 1 \end{bmatrix} \begin{bmatrix} \dot{\gamma}_b \\ \dot{x}_b \\ \dot{y}_b \end{bmatrix} = h_i \boldsymbol{V_b} \tag{4}$$

where $\boldsymbol{p_{P_1}} = [x_i, y_i]^T$ represents the position vector of the $i$-th swerve drive unit center point $P_1$ expressed in the mobile frame $\{b\}$.

Hence, by considering the AGRIMARO.Q layout, the following expression can be derived:

$$\begin{bmatrix} \boldsymbol{s_1}(\delta_1) \\ \boldsymbol{s_2}(\delta_2) \\ \boldsymbol{s_3}(\delta_3) \end{bmatrix} \begin{bmatrix} \dot{\theta}_1 \\ \dot{\theta}_2 \\ \dot{\theta}_3 \end{bmatrix} = \begin{bmatrix} 0 & 1 & 0 \\ w/2 & 0 & 1 \\ 0 & 1 & 0 \\ -w/2 & 0 & 1 \\ t & 1 & 0 \\ 0 & 0 & 1 \end{bmatrix} \begin{bmatrix} \dot{\gamma}_b \\ \dot{x}_b \\ \dot{y}_b \end{bmatrix} \quad \Leftrightarrow \quad S(\boldsymbol{\delta})\, \dot{\boldsymbol{\theta}} = H\, \boldsymbol{V_b} \tag{5}$$

It is worth noting that the mapping here presented straightforwardly allows the forward kinematics computation, that is:

$$\boldsymbol{V_b} = H^{\dagger}\, S(\boldsymbol{\delta})\, \dot{\boldsymbol{\theta}} \tag{6}$$

On the other hand, since the $S$ matrix is configuration-dependent, the inverse kinematics problem cannot be similarly derived.

### 3.1 Operational space velocities under actuation constraints

Although AGRIMARO.Q can be framed as a pseudo-omnidirectional service robot thanks to its three swerve drive units, a real mobile robotic system is usually affected by actuation constraints, that could limit the robot performance. These physical upper limits often regard the wheel rotation speed, the steering speed and the steering angle range; altough the latter does not concern AGRIMARO.Q for the embedding of slip rings within the swerve drive unit executive design.

Regarding the remaining two physical limits, this subsection aims at estimating the behavior of the AGRIMARO.Qmobile platform while affected by wheel speed limitations, thus neglecting the self-reconfiguration time requested to change the instantaneous center of rotation of the chassis [8].
Referring to Eqn. (5), the norm of the $i$-th wheel linear speed $\|\dot{\boldsymbol{p}}_{\boldsymbol{i}}\|$ can be written as:

$$\frac{\|\dot{\boldsymbol{p}}_{\boldsymbol{i}}\|}{\omega_{max}\, r} = \pm \sqrt{\left(\frac{\dot{x}_b}{\omega_{max}\, r} - y_i \frac{\dot{\gamma}_b}{\omega_{max}\, r}\right)^2 + \left(\frac{\dot{y}_b}{\omega_{max}\, r} + x_i \frac{\dot{\gamma}_b}{\omega_{max}\, r}\right)^2} \tag{7}$$

where $\omega_{max}$ is the maximum wheel speed and it is assumed equal for all three wheels. Moreover, the plus-minus sign underlines that, within the interval $\delta_i \in [-\pi, \pi]$, there are two possible solutions of the inverse kinematics problem, i.e. by turning the drive wheel by 180°and by imposing a rotating speed in the opposite direction, the same linear velocity $\|\dot{\boldsymbol{p}}_{\boldsymbol{i}}\|$ can be obtained. The above equation can be now expanded as follows:

$$\Omega_1 = \frac{\|\dot{\boldsymbol{p}}_1\|}{\omega_{max}\, r} = \pm\sqrt{\left(\frac{\dot{x}_b}{\omega_{max}\, r}\right)^2 + \left(\frac{\dot{y}_b}{\omega_{max}\, r} + \frac{w}{2}\frac{\dot{\gamma}_b}{\omega_{max}\, r}\right)^2}$$
$$\Omega_2 = \frac{\|\dot{\boldsymbol{p}}_2\|}{\omega_{max}\, r} = \pm\sqrt{\left(\frac{\dot{x}_b}{\omega_{max}\, r}\right)^2 + \left(\frac{\dot{y}_b}{\omega_{max}\, r} - \frac{w}{2}\frac{\dot{\gamma}_b}{\omega_{max}\, r}\right)^2} \tag{8}$$
$$\Omega_3 = \frac{\|\dot{\boldsymbol{p}}_3\|}{\omega_{max}\, r} = \pm\sqrt{\left(\frac{\dot{x}_b}{\omega_{max}\, r} + t\frac{\dot{\gamma}_b}{\omega_{max}\, r}\right)^2 + \left(\frac{\dot{y}_b}{\omega_{max}\, r}\right)^2}$$

To introduce the wheel speed upper constraints, still under the simplifying assumption of a pure-rolling constraint, it is enough to notice the value on the left-hand side of the equation is bounded above:

$$\|\Omega_i\| < 1 \tag{9}$$

The result of how the limit on the drive wheels speed affects the platform behavior is depicted in Fig. 4 within a dimensionless body twist space that is defined by normalizing $\boldsymbol{V_b}$:

$$\dot{\Gamma}_b = a\frac{\dot{\gamma}_b}{\omega_{max}\, r}\ ,\ \dot{X}_b = \frac{\dot{x}_b}{\omega_{max}\, r}\ ,\ \dot{Y}_b = \frac{\dot{y}_b}{\omega_{max}\, r} \tag{10}$$

with $a = w/2$ and by defining the dimensionless geometric parameter $\xi$ as:

$$\xi = \frac{2t}{w} = \frac{t}{a} \tag{11}$$

The resulting 3D convex polyedhron of the AGRIMARO.Q admissible body twists are displayed in Fig. 4 within the dimensionless space above defined. To get a physical understanding of these results, Fig. 5 shows the contour of the polyhedron with $\dot{Y}_b = 0$ and with $\xi$ ranging between the interval $[0.5, 4]$.

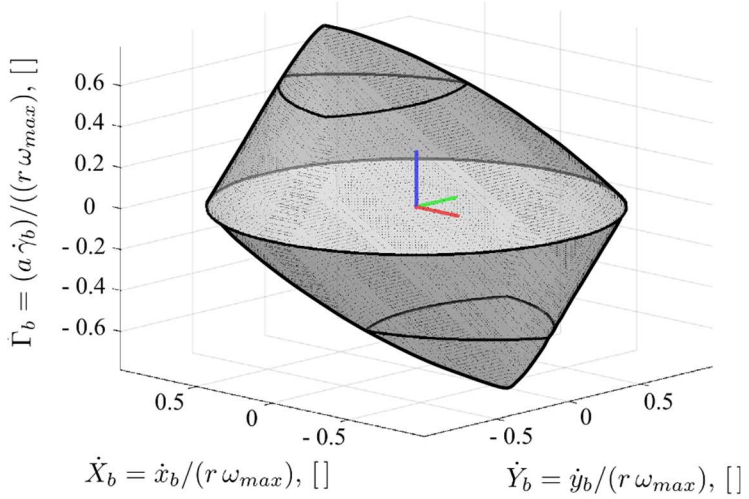


**Fig. 4.** AGRIMARO.Q mobile robot admissible body twists within the dimensionless space $\{\dot{X}_b, \dot{Y}_b, \dot{\Gamma}_b\}$ with $\xi = 2\ t\ /w = 2$.

Since no linear motion along $\hat{v}$ is here considered, the instantaneous center of rotation of the planar motion (i.c.r.) lies on the $\hat{u}$ axis of $\{b\}$. The upper limit condition, here not reported, would have been represented by the case with $\xi \ll 1$, i.e. if the AGRIMARO.Q track had been almost null. In this fashion, the AGRIMARO.Q behavior would have been similar to a 2SWD (two swerve drive) platform, for the first and second wheel would have been equally distant from the i.c.r. and the resulting convex domain is a circle. On the other hand, by increasing the chassis track value $t$, the constraints specified in Eqn. (8) cut the circle with two straight lines whose slope depends on the track value itself. While in $C_1$ the platform is still acting as stated above, in point $C_2$ the i.c.r. is equally distant from all the three drive wheels and, by imposing the maximum allowed wheel speed, the dimensionless yaw angular rate is equal to:

$$\dot{\Gamma}_{b,C_2} = \frac{1}{\xi - \frac{\xi^2-1}{2\,\xi}} \tag{7}$$

From hereon, the third drive wheel becomes the outer wheel and limits the platform body twist. In addition, point $C_3$ represents the condition where no linear motion of

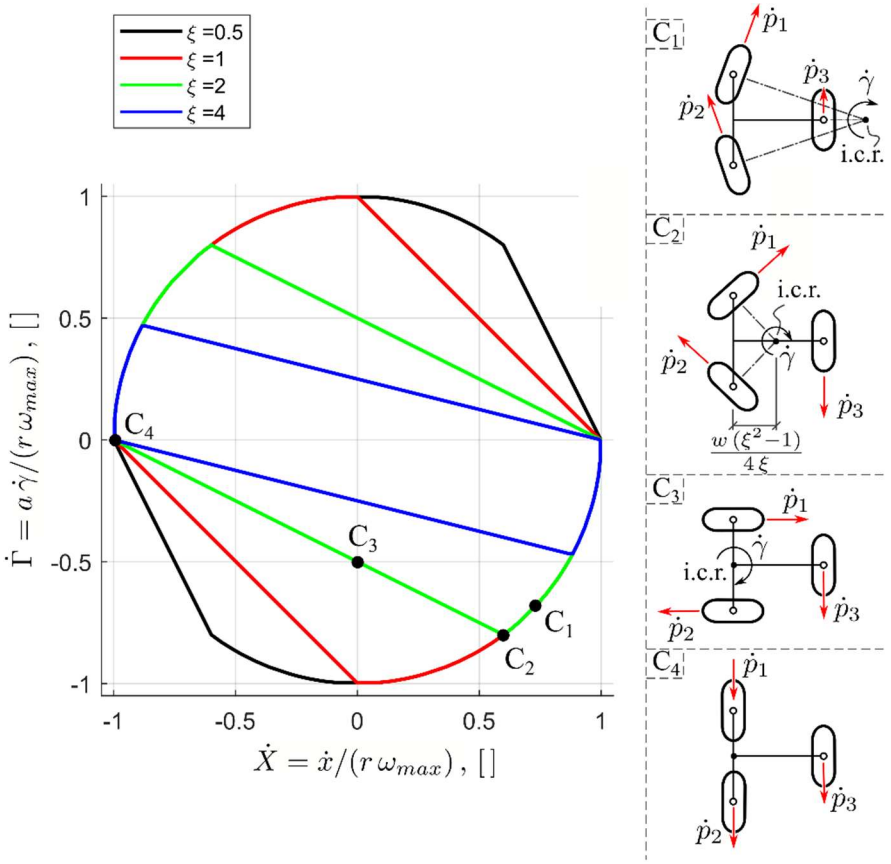


**Fig. 5.** Admissible body twist regions with $\dot{Y}_b = 0$ and different values of $\xi$.

point O is imposed, thus O corresponds to the i.c.r. itself. In this case, the computation of the yaw angular rate is straightforward:

$$\dot{\Gamma}_{b,C_3} = \frac{1}{\xi} \tag{8}$$

The latter case, i.e. point $C_4$, represents a pure translation motion, thus the dimensionless maximum linear speed is merely equal to one.

## 4 Conclusions

The paper presented a novel pseudo-omnidirectional robot for protected cultivation applications, such as fertilizer distribution or crop monitoring. The robot can be framed within the small-medium sized robot, with an overall weight of the mechanical components of approximately 60kg. The paper showed the robot functional and final layout, then presented the kinematic model of the pseudo-omnidirectional platform. In addition, a few considerations about how the actuation constraints limit the robot mobility, especially when performing combined linear and yaw motions, were carried out introducing the AGRIMARO.Q variable track length. The final results provide indications about the behavior of the mobile platform, thus allowing the design of control strategies that prevent from reaching out the allowed body twist polyhedron edges.

**Acknowledgments** This work was supported by the National Center for the Development of New Technologies in Agriculture (Agritech). https://agritechcenter.it/ (accessed on 01 March 2024).

## 5 References

1. Botta, A. *et al.*: A Review of Robots, Perception, and Tasks in Precision Agriculture. Applied Mechanics 3, 830–854 (2022).
2. Van Henten, E. J. *et al.*: Robotics in protected cultivation. In: IFAC Proceedings Volumes, Finland, pp. 170-177 (2013).
3. Arad, B. *et al.*: Development of a sweet pepper harvesting robot. Journal of Field Robotics 37(6), 1027–1039 (2020).
4. Lehnert, C., English, A., McCool, C., Tow, A.W., Perez, T.: Autonomous Sweet Pepper Harvesting for Protected Cropping Systems. IEEE Robotics and Automation Letters 2(2), 872–879 (Apr 2017). https://doi.org/10.1109/LRA.2017.2655622.
5. Birrell, S., Hughes, J., Cai, J.Y., Iida, F.: A field-tested robotic harvesting system for iceberg lettuce. Journal of Field Robotics 37(2), 225–245 (2020). https://doi.org/10.1002/rob.21888
6. Grimstad, L., From, P.J.: The Thorvald II Agricultural Robotic System. Robotics 6(4), 24 (2017). https://doi.org/10.3390/robotics6040024.
7. Eraslan, N.F.: On the synthesis of certain straight-line mechanisms. Mechanism and Machine Theory 14(5), 299–307 (1979). https://doi.org/10.1016/0094-114X(79)90016-8
8. Tagliavini, L. *et al.*: Wheeled Mobile Robots: State of the Art Overview and Kinematic Comparison Among Three Omnidirectional Locomotion Strategies. Journal of Intelligent & Robotic Systems, 106, 57 (2022).